



MIT Open Access Articles

Frequency-based current-sharing techniques for paralleled power converters

The MIT Faculty has made this article openly available. **Please share** how this access benefits you. Your story matters.

Citation	Perreault, D.J., R.L. Selders, and J.G. Kassakian. "Frequency-Based Current-Sharing Techniques for Paralleled Power Converters." IEEE Trans. Power Electron. 13, no. 4 (July 1998): 626–634.
As Published	http://dx.doi.org/10.1109/63.704128
Publisher	Institute of Electrical and Electronics Engineers (IEEE)
Version	Final published version
Citable link	http://hdl.handle.net/1721.1/86877
Terms of Use	Article is made available in accordance with the publisher's policy and may be subject to US copyright law. Please refer to the publisher's site for terms of use.

Frequency-Based Current-Sharing Techniques for Paralleled Power Converters

David J. Perreault, *Member, IEEE*, Robert L. Selders, Jr., and John G. Kassakian, *Fellow, IEEE*

Abstract— A new current-sharing technique for paralleled power converters, which is based on frequency encoding of the current-sharing information, is introduced. The approach has significant advantages over existing methods, including the ability to transformer isolate or eliminate current-sharing control connections. Operation of the current-sharing technique is analyzed, and the design and experimental evaluation of a three-cell prototype system are presented.

Index Terms—Cellular, current sharing, load sharing, modular, parallel.

I. INTRODUCTION

POWER conversion systems are sometimes constructed by paralleling converters in order to improve performance or reliability or to attain a high system rating. A desirable characteristic of a parallel converter architecture is that the individual converters share the load current equally and stably. The current-sharing behavior of the system is largely dependent on the manner in which the individual converters are controlled. Many parallel converter systems use some form of global control in which a single, possibly redundant, controller directly regulates the load balance among the individual converters [1]–[10]. However, to enhance modularity and improve reliability, it is more desirable to have the load-sharing control distributed among the converters. This is especially true in *cellular* converter architectures in which large numbers of quasi-autonomous converters, called *cells*, are paralleled to form a large power converter [11]–[13].

In order to implement a distributed load-sharing scheme, only a very limited amount of information needs to be shared among the individual cells. For example, given information about the average cell output current, each cell can regulate its output to be close to the average [14]–[21]. Other quantities valid for the ensemble of converter cells can also be used, including rms cell current [22], weighted cell current stress [23], and highest cell current [24].

Load-sharing information is most commonly generated and shared over a single interconnection among converter cells. Typically, the interconnection circuit is designed so that when

each cell generates a signal proportional to its output, the voltage on the interconnection bus is the average (or maximum, etc.) of the individual signals. For ac-output converters, the interconnection may sometimes be transformer isolated from the local cell control circuits [14], [15]. However, for many applications, transformer isolation cannot be employed using conventional methods since the current-sharing information has frequency content down to dc.

Approaches exist where current-sharing information is communicated implicitly via the output, and no additional interconnections among converter cells are required. For paralleled constant-frequency inverters, load balance can be achieved by implementing a frequency and voltage droop characteristic in each cell output. This technique, which is also used to regulate the power output of paralleled generators in an ac supply system, basically employs the ac bus voltage and frequency to communicate power-sharing information among the controllers [15], [25]. Unfortunately, the complexity and cost of the approach limits its use to relatively large inverter cells. The dc-output power supplies sometimes use output-voltage droop characteristics to achieve a degree of current sharing [9], [26], [27]. While simple, this approach yields heavy load regulation in the output and steady-state current imbalances, which are often unacceptable.

This paper introduces a new frequency-domain-based method for encoding and distributing current-sharing information among cells. This new scheme has significant advantages over existing methods, particularly with respect to reliability. It operates in the following manner. Each converter cell generates a (typically sinusoidal) signal whose frequency is related to the average output current (or power or other variable to be regulated) of the cell. The signal frequency range used can be widely separated from the fundamental output frequency of the converter system. The signals from each cell are summed, with the result available to each cell. Each cell employs a frequency estimator circuit to calculate a weighted average ω_{est} of the frequency content of the aggregate signal. Each cell can then compare its own generated frequency ω_k to the weighted average ω_{est} and adjust its output to make $\omega_k \simeq \omega_{est}$. With this method, *a priori* information about the number of cells in a paralleled system is unnecessary since each cell needs only the aggregate signal for current sharing to be effected. Thus, current sharing is preserved even if cells fail or are added.

This frequency encoding approach circumvents some of the major limitations of existing current-sharing methods. The direct interconnection among control circuits present in conventional distributed load-sharing schemes is a source of

Manuscript received October 18, 1996; revised October 14, 1997. This work was supported by the Bose Foundation and the United States Office of Naval Research. Equipment grants were supported by the Intel and Tektronix Corporations. D. J. Perreault was supported by an IEEE Convergence Fellowship in Transportation Electronics. R. L. Selders, Jr. was supported by Delco Electronics under the Delco Electronics Scholarship Program. Recommended by Associate Editor, A. Kawamura.

The authors are with the Laboratory for Electromagnetic and Electronic Systems, Massachusetts Institute of Technology, Cambridge, MA 02139 USA. Publisher Item Identifier S 0885-8993(98)04845-5.

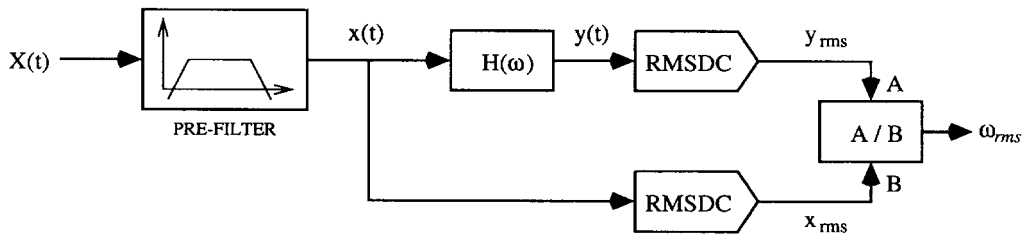


Fig. 1. An approach for calculating the weighted rms frequency estimate of the aggregate signal. This approach is easily implemented in analog or digital hardware.

single-point failure mechanisms which, in the worst case, can bring the entire converter system down. Elimination of single-point failure modes is a key design objective for achieving fault tolerance in distributed converter architectures [28]. We will show that with the frequency-based approach, current-sharing information can be encoded at high frequencies and distributed over the output or input bus, making additional control interconnections among cells unnecessary. Alternatively, if separate interconnections for current sharing are used, they may be galvanically isolated using small high-frequency transformers. Thus, the frequency encoding method allows improvements in reliability and availability by eliminating the failure modes associated with direct interconnections among the control circuits.

This new control design has other potential advantages. In conventional schemes, current-sharing information is encoded and distributed at low frequencies (typically down to dc). With the frequency-encoding approach, the designer can select the frequency range over which current-sharing information is communicated and can use this design freedom to achieve objectives such as noise minimization. Furthermore, with the frequency-based method, the aggregate current-sharing signal contains information about the total number of converter cells and their *individual* output currents in addition to information about the average output of the converters. This may have some benefits for system monitoring and fault detection.

II. FREQUENCY ESTIMATION

To reduce this new current-sharing approach to practice, a means of estimating an average frequency ω_{est} from the aggregate signal using simple inexpensive circuitry is needed. Many different types of weighted estimates and estimator structures are possible. This section considers the implementation of an rms frequency estimator although other frequency-based estimation and control schemes exist which are also well suited to the task.

Consider the aggregate current-sharing signal $x(t)$, which is made up of a group of N sinusoids $x_k(t)$ of frequencies ω_k , $k = 1, \dots, N$. The frequency of an individual sinusoid encodes information about the output current of a particular cell, while the rms frequency of the aggregate signal can be used to effect current-balancing control. The weighted rms frequency for all of the sinusoids is defined as

$$\omega_{\text{rms}} = \frac{\sqrt{\sum_{k=1}^N c_k^2 \omega_k^2}}{\sqrt{\sum_{k=1}^N c_k^2}} \quad (1)$$

where the c_k 's are weighting coefficients for different frequencies. For equal weighting, the c_k 's can be considered equal to a single (arbitrary) constant. The power spectrum of $x(t)$ is

$$S_x(\omega) = 2\pi \sum_{k=1}^N \frac{1}{2} |X_k|^2 [\delta(\omega - \omega_k) + \delta(\omega + \omega_k)] \quad (2)$$

where we have assumed that all of the $x_k(t)$'s are at separate frequencies. The violation of this assumption affects the weightings in the rms frequency estimate, but does not interfere with the overall operation of the current-sharing system. The rms value of $x(t)$ is then

$$x_{\text{rms}} = \sqrt{\frac{1}{2\pi} \int_{-\infty}^{+\infty} S_x(\omega) d\omega} = \sqrt{\sum_{k=1}^N |X_k|^2}. \quad (3)$$

If we pass the signal $x(t)$ through a filter with frequency response $H(\omega)$ to form a signal $y(t)$, we find the new signal $y(t)$ has the properties

$$S_y(\omega) = 2\pi \sum_{k=1}^N \frac{1}{2} |H(\omega_k)|^2 |X_k|^2 [\delta(\omega - \omega_k) + \delta(\omega + \omega_k)] \quad (4)$$

and

$$y_{\text{rms}} = \sqrt{\frac{1}{2\pi} \int_{-\infty}^{+\infty} S_y(\omega) d\omega} = \sqrt{\sum_{k=1}^N |H(\omega_k)|^2 |X_k|^2}. \quad (5)$$

Now, consider the estimator implementation shown in Fig. 1. If we choose the filter $H(\omega)$ to be a differentiator over the encoding frequency range ($H(\omega) = j\omega$), we find that the ratio of the rms value of $y(t)$ to the rms value of $x(t)$ has the form of the desired rms frequency estimate (1), with the signal magnitudes as the weighting coefficients. This result means that the desired rms frequency estimate can be easily computed using simple analog or digital hardware. The rms frequency estimate can be calculated with analog circuitry using two (integrated circuit) rms-to-dc converters, a differentiator, and a divider. Alternately, the estimate can be computed digitally by sampling $x(t)$ and performing the equivalent calculations in software. These results have been derived for computations on fixed-frequency signals over all time. However, computation of these rms quantities over a sliding window allows the frequency content (and hence the current-balance information) to be tracked over time. Appendix A addresses the use of practical rms-to-dc converters for this purpose and shows the effects of the averaging time constant of the rms-to-dc converters on frequency resolution and response speed.

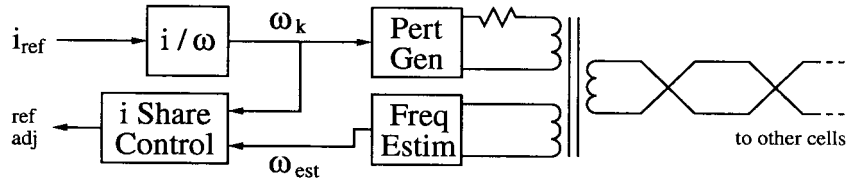


Fig. 2. Schematic of the isolated single-connection implementation of frequency-based load-sharing control.

We conclude from these results that if the individual cells encode information about their output current in the frequency of a signal, then information about the average output of all the cells can be easily extracted from the aggregate signal with very simple hardware. We now employ these results to implement the new frequency-based current-sharing scheme.

III. IMPLEMENTATION APPROACHES

To implement load-sharing control using the frequency encoding method, the signals from the individual cells are summed at a node, and the sum is accessible to all the cells. There are several ways to do this. We will consider three of them: 1) the isolated single-connection implementation; 2) the output perturbation implementation; and 3) the switching ripple implementation.

A. The Isolated Single-Connection Implementation

The *isolated single-connection implementation*, shown in Fig. 2, communicates current-sharing information over a dedicated bus, similar to existing single-connection approaches [14]–[21], [23], [24]. Each converter cell injects onto the current-sharing bus a signal whose frequency is related to its output current. The cell measures the aggregate signal on the bus to determine ω_{est} and control current balance. Transformer isolation can be employed because there is no low-frequency content to the current-sharing signals. Transformer isolation reduces the possibility that a single-point failure can damage the whole system via the current-sharing connections. Furthermore, this approach is advantageous for systems in which the converter control circuits do not share a common ground, such as isolated converter cells supplied from different power sources.

B. The Output Perturbation Implementation

The *output perturbation implementation* shown in Fig. 3 uses small sinusoidal perturbations in the cell output currents to encode current-sharing information. Each cell computes an estimate (using the same method as the isolated single connection implementation) of the average output of all cells from the resulting aggregate perturbation in output voltage, which is locally measurable by each cell. This information is then used to achieve load balance among cells. The perturbation frequency range is typically selected to be well above the output-voltage control bandwidth of the system, but well below the switching frequency. The needed perturbations in output current are easily generated in converters under current-mode control, and only very small perturbations in output current (and voltage) are necessary to communicate current-

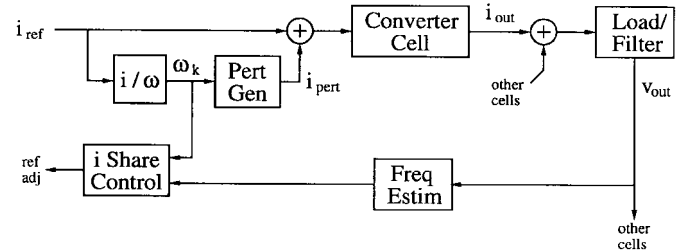


Fig. 3. Schematic of the output perturbation implementation of frequency-based load-sharing control.

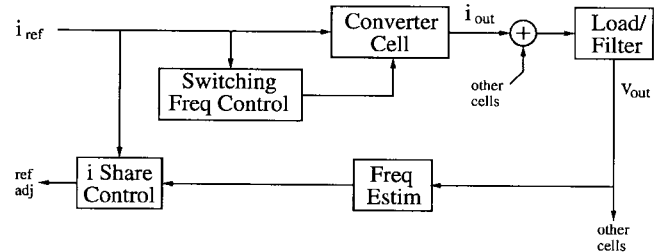


Fig. 4. Schematic of the switching-frequency implementation of frequency-based load-sharing control.

sharing information. The output perturbation implementation achieves current balance control using only variables measured locally at each converter cell, with no intercell connections for current sharing. No additional power processing components or sensors are needed to communicate the current-sharing information across the output bus. This yields a potential reliability advantage over systems which require additional interconnections.

The use of the output bus to communicate current-sharing information has other interesting characteristics. For example, conditions which disrupt the distribution of current-sharing information (such as output short circuits) generally cause enough of a voltage error to drive all of the converters to full current, making current sharing temporarily unnecessary. Furthermore, faults in an individual cell which cause it to be removed from operation (such as by the output fuse blowing) automatically prevent it from affecting current sharing among the remaining converter cells. These characteristics yield a current-sharing approach which is potentially very robust. The major challenge to implementing the approach is the selection of an appropriate perturbation magnitude and frequency range.

C. The Switching Ripple Implementation

The *switching ripple implementation* shown in Fig. 4 is similar to the output perturbation method, except that the

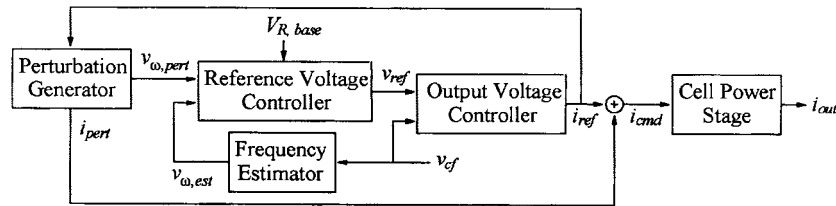


Fig. 5. Block diagram of the control structure for a cell.

switching ripple of the cell is used as the perturbation source. Each converter cell is controlled such that its average output current (or some other variable to be regulated) is directly related to its switching frequency. Each converter can locally measure the aggregate switching harmonics at the output and use the information in the switching harmonics to achieve load balance with the other converter cells. This approach has the benefit that no additional ripple is injected into the output to encode current sharing information, and the information is communicated at the switching frequency (i.e., with high bandwidth).

Controlling the switching frequency of the converters is typically straightforward. For many converter types, there is a natural relation between switching frequency and control variables such as output current. Converter control strategies which do not exhibit such a relation can often be modified to achieve it. For example, such a relationship can be implemented in fixed-frequency pulsewidth modulation (PWM) converters by modifying the clock frequency as a function of output current.

Estimating an average value for the current (or frequency, or other control variable) from the aggregated output harmonics is a more delicate task. Because the switching harmonic content of a single converter operating at any frequency/current is known, information about the average can clearly be extracted from the output voltage. However, the existence of (possibly large) harmonics of the fundamental ripple current from each cell makes the estimation task more complicated than that for the output perturbation method. Nevertheless, we have managed to verify that for some converter types it is possible to estimate the rms output current directly from the net switching ripple using only locally measurable variables [29]. Furthermore, some very simple estimation and control structures exist which are insensitive to harmonic components and are thus well suited to the switching-ripple implementation [30].

IV. PROTOTYPE SYSTEM

A low-power three-cell prototype converter system using the output perturbation method was constructed. Here, we describe the implementation of the prototype system, which employs low-power buck converter cells operating under current-mode control. In simplest terms, each cell can be viewed as having an inner current control loop, a middle voltage control loop, and an outer load-sharing control loop. Implementation of the outermost loop with the perturbation method requires that each cell encode information about its current onto the output (via a perturbation generator) and decode the aggregated information from the output (via a frequency estimator). We will describe

methods and circuits for generating the proper perturbation signals, estimating the rms perturbation frequency from output-voltage measurements, and controlling the load balance among cells.

The structure of an individual cell implementing the perturbation method is shown in Fig. 5. The converter cell power stage generates an output current whose peak value is equal to the peak commanded current i_{cmd} . The commanded current is the sum of a reference current i_{ref} , generated by the output-voltage controller, and a perturbation signal i_{pert} , generated by the perturbation generator circuit. The output-voltage controller generates i_{ref} based on the difference between the output voltage v_{cf} and the reference voltage v_{ref} . The load-sharing controller adjusts v_{ref} based on the difference between the local perturbation frequency and the rms perturbation frequency calculated by the frequency estimator circuit. These subsystems operate together to regulate the output voltage while maintaining the desired load balance among cells.

A. Prototype System Power Stage

A three-cell low-power buck converter system was constructed as a test bed. The buck converter cells ($f_{sw} \simeq 200$ kHz and $L \simeq 125$ mH) are designed to regulate the output to an adjustable reference of approximately 5.1 V from an input voltage of approximately 15 V. The individual cells are designed to supply a full load output current of 25 mA, yielding a total load range of 5–75 mA. The system has an output filter capacitance of 0.33 μ F and is resistively loaded.

The individual cells are operated under current-mode control using the UC3843 current-mode control chip. The internal current-sense comparator and error amplifier are overridden and replaced with external circuitry to allow direct control of the commanded peak turn-off current i_{cmd} .

B. Perturbation Generation

The prototype perturbation generator circuit implements an incrementally linear relationship between cell reference current and perturbation frequency, with cell currents from no load to full load yielding perturbation frequencies from 5 to 10 kHz. The perturbation frequency range is selected to be well below the 200-kHz cell switching frequency, but well above the output-voltage control bandwidth of the system (~ 100 Hz). The perturbation magnitude is selected to be proportional to the perturbation frequency, with a maximum magnitude of approximately 0.25 mA at 10 kHz. This is done to yield output-voltage perturbations (across the capacitive output filter), which are approximately constant in magnitude

across frequency. The selected magnitude range yields very small (<1%) output-voltage ripple for the three-cell system.

The perturbation generator is implemented using an XR2206 monolithic function generator, which contains a voltage-controlled oscillator (VCO) and sine-wave-shaping circuitry. The VCO input allows control of the perturbation frequency, and an amplitude modulation input allows easy control of the perturbation magnitude. The generated perturbation signal is superimposed on the reference current, and the result is supplied to the current-mode PWM controller.

C. Frequency Estimation

To achieve load balance, each cell compares its own perturbation frequency to the rms of all the perturbation frequencies. The rms perturbation frequency is estimated from the output voltage using the structure of Fig. 1, with $H(\omega) = j\omega$. The estimator is composed of four sections: 1) a bandpass filtering stage; 2) a gain and band-limited differentiation stage; 3) an integrated circuit rms-to-dc conversion stage; and 4) a division stage. The bandpass filtering stage is implemented as a cascade of a second-order high-pass Butterworth filter, a fixed gain, and a second-order low-pass Butterworth filter. The corner frequencies are set to 500 Hz and 20 kHz in order to block out both the low-frequency and switching-frequency components of the output voltage. The differentiation stage consists of a band-limited differentiator circuit which generates the derivative for frequency components in the range of interest, but is gain limited above approximately 50 kHz to limit the amplification of high-frequency noise. The rms-to-dc conversion stage is implemented using AD637 integrated circuit rms-to-dc converters connected in the two-pole Sallen–Key filter arrangement. The averaging and filter capacitor values ($C_{AV} = 0.022 \mu\text{F}$ and $C_2 = C_3 = 0.047 \mu\text{F}$) are selected to yield a 1% settling time of 8 ms, which represents a reasonable tradeoff between frequency resolution and response speed (see Appendix A for an analysis of this tradeoff). The division stage is composed of a four-quadrant multiplier placed in the feedback path of an operational amplifier. This approach is typically less expensive than the use of a logarithm-based division circuit, but requires careful attention to the compensation of the nonlinear feedback loop. The division stage also incorporates an output scale and offset compensation circuit for improved accuracy. The prototype estimator employs only simple low-cost circuitry and has sufficient accuracy to achieve a high degree of current sharing.

D. Control Design

For the parameters of the prototype system, an individual cell under peak current-mode control can be modeled as a controlled current source of the value of the peak commanded current. To achieve output-voltage control, a high-gain single-pole compensator (Gain = 125 and mA/V, $\tau = 0.18$ s) is used to generate the peak control current from the error between the reference voltage and output voltage. This yields an output-voltage control bandwidth on the order of tens of hertz and a small, but nonzero cell output impedance.

Load balance among cells is controlled by adjusting the local cell reference voltages within limits about a base value. Each cell has a high-gain single-pole compensator (Gain = 10 V/kHz and $\tau = 33.6$ s), which generates a reference voltage adjustment based on the difference between the estimated rms perturbation frequency and the cell perturbation frequency (Fig. 2). This yields a load-sharing bandwidth on the order of hertz (much slower than the voltage control loop) and a small, but nonzero steady-state load-sharing error.

V. EXPERIMENTAL RESULTS

Here, we evaluate the new load-sharing control approach using a three-cell prototype system of the presented design. Fig. 6 shows the load-sharing behavior at approximately 60% load both with and without the load-sharing control. Without load-sharing control, a 3:2 imbalance between the highest and lowest cell currents is observed, with much worse imbalances sometimes occurring depending on the individual cell reference voltages and output impedances. With load-sharing control, the cell currents are all balanced within 3% of their average. (We point out that the perturbation method yields accurate load-sharing *regardless* of how the cells share current without active control.) This high degree of load sharing is achieved using only very small (<1%) perturbations in output voltage to encode current-sharing information (Fig. 7).

Fig. 8 shows the static load-sharing behavior of the system over the whole load range, while Fig. 9 shows the load regulation characteristic of the converter system over the load range. The load sharing is quite good over the entire range, but is better at heavier loads both in absolute terms and as a percent of total current. (We point out that while good current sharing is desirable over the whole load range, it is much more important at heavier loads, where the cells are under higher stress.) Current sharing limitations are primarily due to the accuracy of the frequency estimators and the perturbation generators. The frequency estimator circuits have an absolute accuracy of about ± 250 Hz over the 5–10-kHz range, which corresponds to an absolute current error of about ± 1.25 mA. This maximum absolute error becomes more significant as a percentage at lighter loads. Furthermore, the estimators tended to be more accurate at frequencies above 8 kHz, leading to smaller absolute errors at heavier loads. Nevertheless, these results demonstrate that accurate static current sharing can be obtained over a wide load range with this approach.

Load-sharing behavior was also investigated under transient conditions. Fig. 10 shows the current-sharing behavior for load steps between 681 and 74 Ω , corresponding to approximately 10% and 100% of full load. (Fig. 11 shows the frequency spectrum of the output-voltage perturbations used to achieve current sharing at these load values.) The current-sharing behavior is seen to be very stable for even large load steps. Fig. 12 shows the response to a current-sharing disturbance for two cells operating at approximately 30% of full load. The dynamic response to current-sharing errors is also seen to be well behaved. What may be concluded from these results is that the presented output perturbation method can be used to achieve accurate static and dynamic load sharing without the need for additional interconnections among cells.

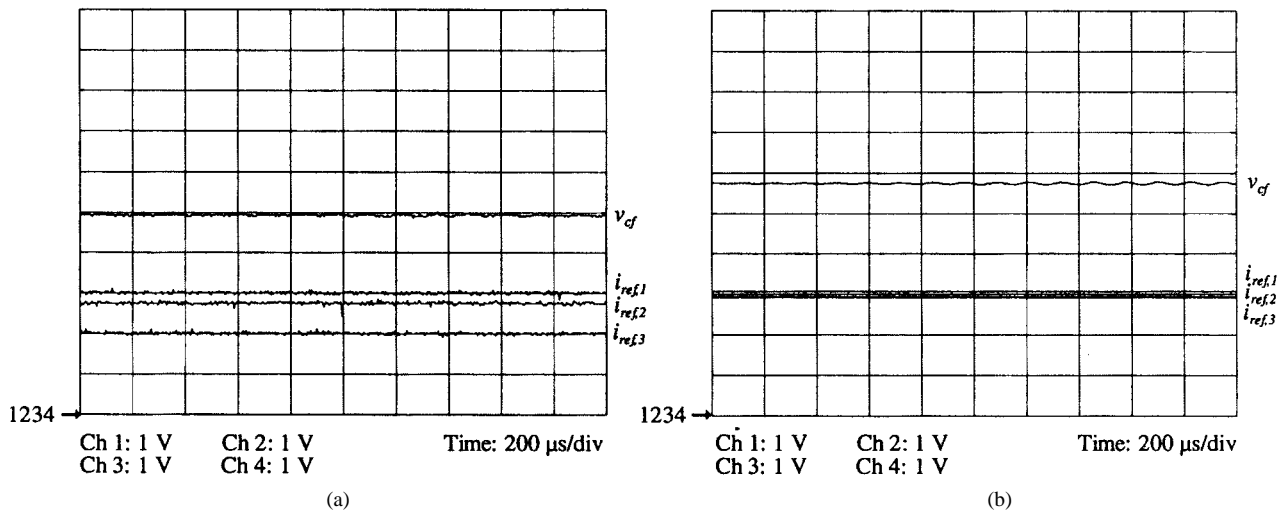


Fig. 6. Load-sharing characteristics of the prototype system at approximately 60% of full load ($R_{load} \approx 133 \Omega$). (a) Without load-sharing control. (b) With load-sharing control.

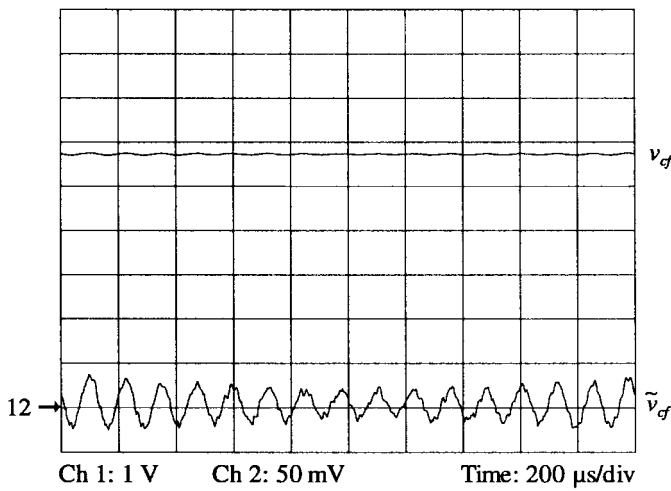


Fig. 7. The output voltage and its ac perturbation component at approximately 60% of full load.

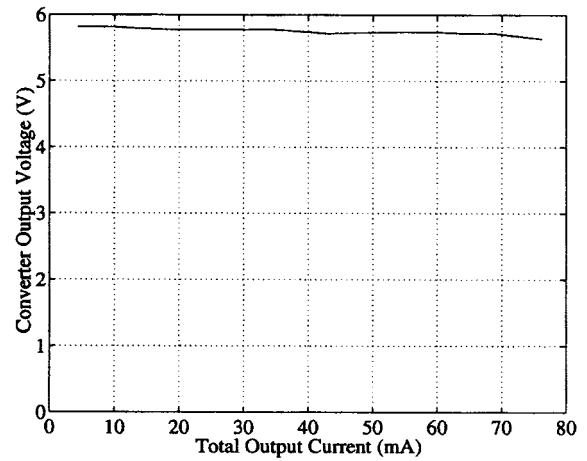


Fig. 9. Load-regulation characteristic of the prototype system.

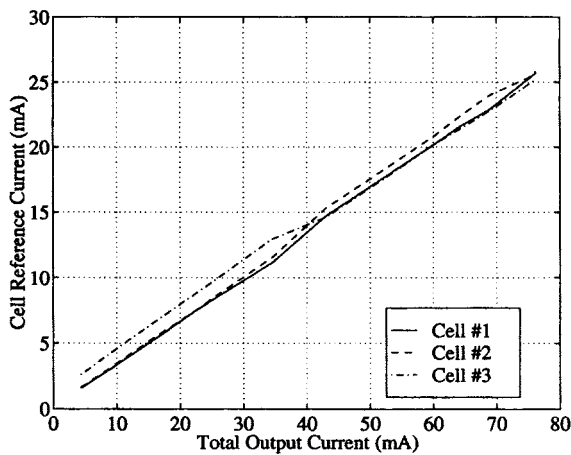


Fig. 8. Static load-sharing characteristic of the prototype system.

VI. CONCLUSION

This paper has presented a new method for achieving current sharing among paralleled converters, based on fre-

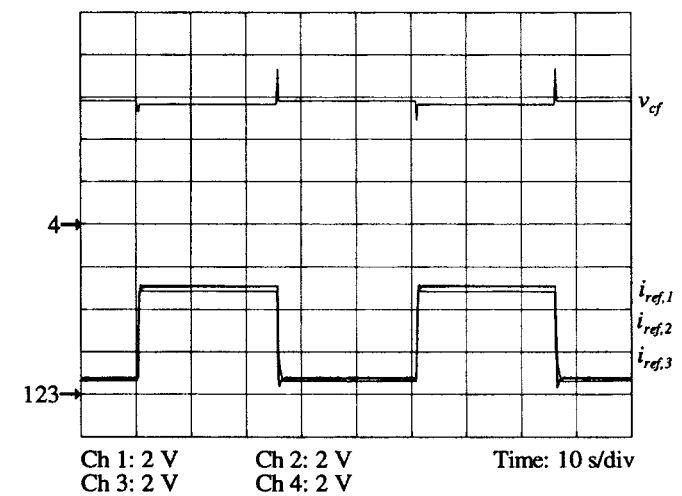


Fig. 10. Current-sharing behavior for load steps between 681 and 74 Ω (approximately 10% and 100% of full load).

quency encoding of the needed information. The current-sharing approach has been analyzed, and different implementation methods have been described. We have shown that

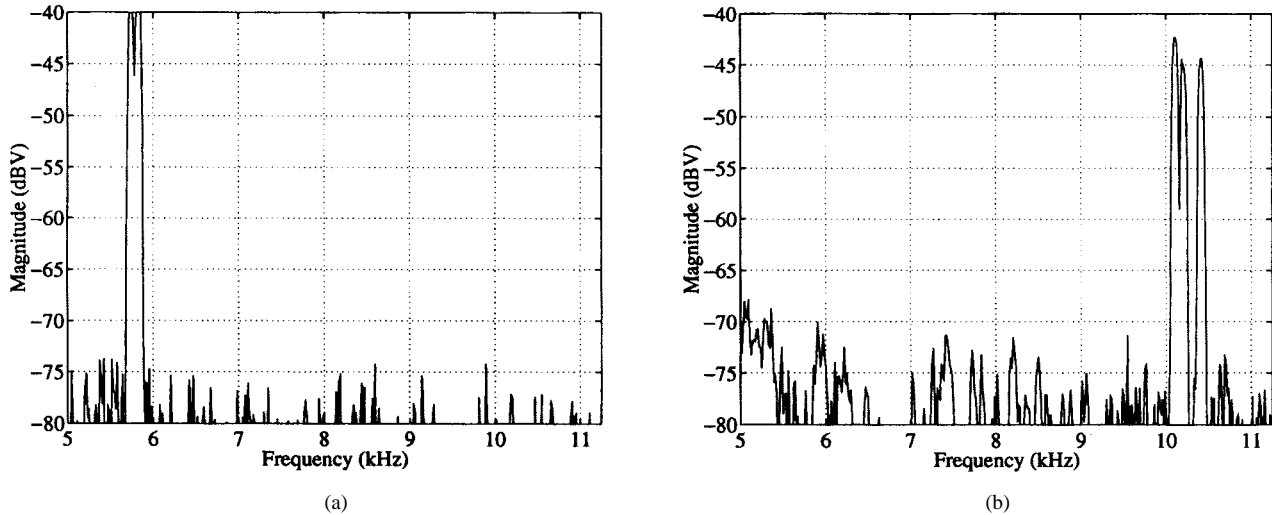


Fig. 11. Frequency spectra of the output-voltage perturbations used to achieve load sharing. (a) $R_{\text{load}} = 681 \Omega$ (approximately 10% of full load). (b) $R_{\text{load}} = 74 \Omega$ (approximately 100% of full load).

the new approach has significant advantages over existing methods, including the ability to galvanically isolate or eliminate the current-sharing connections among cells and the freedom to select the frequency range over which information is communicated. The design of a low-power experimental prototype has been presented, along with experimental results demonstrating the practicality of the method. This converter system achieves very accurate current sharing using very simple load-sharing circuitry and with no additional interconnections among cells.

In conclusion, we would like to point out that other approaches to current sharing are possible which are similar to those presented here and share some of the same advantages. For example, encoding and communicating current-sharing information on the *amplitudes of fixed-frequency* (and phase) signals can be employed to achieve galvanic isolation of current-sharing control circuits. Alternatively, frequency encoding of variables other than current or use of other estimation and control structures may sometimes be desirable. It may be expected that frequency encoding and similar approaches to current sharing will have advantage whenever fault tolerance and high reliability are important system requirements.

APPENDIX A RMS-TO-DC CONVERSION

This Appendix addresses the application of practical rms-to-dc converters to the computations outlined in the paper. Most integrated circuit rms-to-dc converters either explicitly or implicitly calculate the rms of a signal $f(t)$ as

$$f_{\text{rms}}(t) = \sqrt{\text{LPF}\{f^2(t)\}} \quad (6)$$

where LPF denotes a low-pass filtering operation, typically using a first- or second-order filter. We will focus on the effects of computing the mean square using this technique—the rms value is merely the square root of this. We define the weighted

mean square of a signal $f(t)$ with respect to a weighting (or windowing) function $w(t)$ as

$$f_{\text{wms}} = \frac{\int_{-\infty}^{\infty} [w(\tau)f(\tau)]^2 d\tau}{\int_{-\infty}^{\infty} w(\tau)^2 d\tau}. \quad (7)$$

For the conventional mean-square value f_{ms} , we use the weighting function

$$w_T(\tau) = \begin{cases} 1, & -\frac{T}{2} < \tau < \frac{T}{2} \\ 0, & \text{otherwise} \end{cases} \quad (8)$$

and take the limit as $T \rightarrow \infty$, which yields

$$f_{\text{ms}} = \lim_{T \rightarrow \infty} \frac{1}{T} \int_{-\frac{T}{2}}^{\frac{T}{2}} f(\tau)^2 d\tau. \quad (9)$$

Now, consider calculating the “computed mean square” of a signal $f(t)$ using a first-order Butterworth filter with time constant τ_1 . This filter has an impulse response

$$h(t) = \frac{1}{\tau_1} e^{-t/\tau_1} u(t) \quad (10)$$

which yields a computed mean square of $f(t)$

$$\begin{aligned} f_{\text{cms}}(t) &= f^2(t) * h(t) \\ &= \frac{1}{\tau_1} \int_{-\infty}^t e^{(\tau-t)/\tau_1} f^2(\tau) d\tau \\ &= \frac{1}{\tau_1} \int_{-\infty}^{\infty} [e^{(\tau-t)/(2\tau_1)} u(t-\tau) f(\tau)]^2 d\tau. \end{aligned} \quad (11)$$

Examining the form of the last line of (11), it is easily shown that $f_{\text{cms}}(t)$ is equivalent to the weighted mean-square computation (7), with weighting function

$$w_c(\tau) = e^{(\tau-t)/(2\tau_1)} u(t-\tau). \quad (12)$$

The fact that the weighting function is zero for values of τ

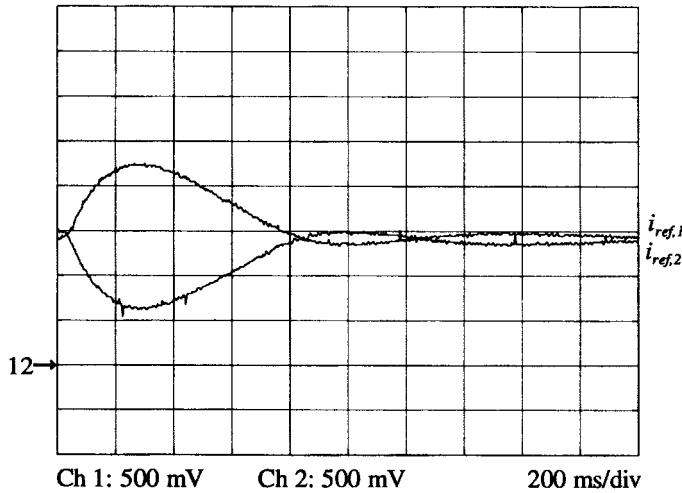


Fig. 12. Dynamic response to a current-sharing perturbation for two cells operating at approximately 30% of full load.

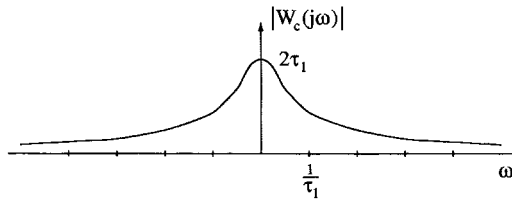


Fig. 13. Frequency response magnitude plot for the weighting function of (12).

greater than t makes physical sense since computations in the actual circuit can only be based on past values of the input signal. This weighting function places a weight of one on the present value of the input signal, with weights for past times decaying exponentially to zero with time constant $2\tau_1$. Thus, the longer the time constant $2\tau_1$, the more heavily the past values of the input signal are weighted and the slower the system responds to changes in the input.

The impact of computing the mean square as in (11) can also be examined from a frequency resolution point of view. This is important since mean-square computations in the frequency-encoding method are typically made on signals composed of closely spaced discrete frequency components. Applying Parseval's relation to (7), we find

$$f_{\text{wms}} = \frac{1}{(2\pi)^2 E_w} \int_{-\infty}^{\infty} |W(j\omega) * F(j\omega)|^2 d\omega \quad (13)$$

where E_w is the energy in the weighting function $w(t)$. From the frequency domain point of view, the mean square reflects the true content of $F(j\omega)$ to the extent that its content is not changed by convolution with $W(j\omega)$. The Fourier transformation of the conventional weighting function from (8), $W_T(j\omega)$, is a sinc function with mainlobe width $\Delta\omega = 2\pi/T$. Thus, the conventional mean-square calculation accurately reflects the spectral content of $f(t)$ to within a resolution of approximately $2\pi/T$ and resolves frequencies with arbitrary accuracy as $T \rightarrow \infty$.

We now consider practical computation of the mean square using the weighting function of (12), which has the transform

$$W_c(j\omega) = \frac{2\tau_1 e^{-j\omega t}}{1 - j2\tau_1\omega} \quad (14)$$

where τ is treated as time and t is a constant parameter. The magnitude of this weighting function frequency response is plotted in Fig. 13. From this, we see that the effect of the weighting function is to "smear" the spectral content of $F(j\omega)$ by an amount depending on τ_1 . There will be significant overlap and loss of resolution among spectral components of $F(j\omega)$ which are closer than roughly $3/\tau_1$ to $5/\tau_1$ apart. The spectral smearing caused by the weighting function affects the computation of the mean square and limits the frequency resolution of a practical estimator.

Thus, practical rms-to-dc converters of the type (6) allow changes in spectral content to be tracked across time, while limiting the frequency resolution of the computation. Both tracking response speed and frequency resolution are controlled by the filter time constant τ_1 and must be traded off against one another in the design process. Similar design issues can be expected to arise in other approaches to the problem, such as with the use of higher order filters or with discrete-time implementations of the mean-square computation.

REFERENCES

- [1] M. Hashii, K. Kousaka, and M. Kaimoto, "New approach to a high power PWM inverter for ac motor drives," in *IEEE Industry Applications Soc. Annu. Meet.*, 1985, pp. 467-472.
- [2] H. Huisman and B. Gravendeel, "A modular and versatile control method for phase-staggering multiple power converters," in *European Power Electronics Conf.*, 1989, pp. 959-963.
- [3] K. Siri, C. Lee, and T. Wu, "Current distribution control for parallel connected converters: Part I," *IEEE Trans. Aerosp. Electron. Syst.*, vol. 28, no. 3, pp. 829-840, 1992.
- [4] F. Petruzzello, P. Ziogas, and G. Joos, "A novel approach to paralleling of power converter units with true redundancy," in *IEEE Power Electronics Specialists Conf.*, 1990, pp. 808-813.
- [5] J. Holtz, W. Lokzat, and K. Werner, "A high-power multitransistor-inverter uninterruptible power supply system," *IEEE Trans. Power Electron.*, vol. 3, no. 3, pp. 278-285, 1988.
- [6] J. Holtz and K. Werner, "Multi-inverter UPS system with redundant load sharing control," *IEEE Trans. Power Electron.*, vol. 37, no. 6, pp. 506-513, 1990.
- [7] J. Chen and C. Chu, "Combination voltage-controlled and current-controlled PWM inverters for UPS parallel operation," *IEEE Trans. Power Electron.*, vol. 10, no. 5, pp. 547-558, 1995.
- [8] S. J. Chiang, C. M. Liaw, W. C. Chang, and W. Y. Chang, "Multi-module parallel small battery energy storage system," *IEEE Trans. Energy Conversion*, vol. 11, no. 1, pp. 146-154, 1996.
- [9] J. Dixon and B. Ooi, "Series and parallel operation of hysteresis current-controlled PWM rectifiers," *IEEE Trans. Ind. Applicat.*, vol. 25, no. 4, pp. 644-651, 1989.
- [10] S. Okuma, K. Iwata, and K. Suzuki, "Parallel running of GTO PWM inverters," in *IEEE Power Electronics Specialists Conf.*, 1984, pp. 111-120.
- [11] J. G. Kassakian, "High frequency switching and distributed conversion in power electronic systems," in *6th Conf. Power Electronics and Motion Control (PEMC'90)*, Budapest, Hungary.
- [12] J. G. Kassakian and D. J. Perreault, "An assessment of cellular architectures for large converter systems," in *1st Int. Conf. Power Electronics and Motion Control*, Beijing, China, 1994, pp. 70-79.
- [13] D. Perreault, J. Kassakian, and H. Martin, "A soft-switched parallel inverter architecture with minimal output magnetics," in *1994 IEEE Power Electronics Specialists Conf.*, Taipei, Taiwan, pp. 970-977.
- [14] L. Walker, "Parallel redundant operation of static power converters," in *IEEE Industry Applications Soc. Ann. Meet.*, 1973, pp. 603-614.

- [15] T. Kawabata and S. Higashino, "Parallel operation of voltage source inverters," *IEEE Trans. Ind. Applicat.*, vol. 24, no. 2, pp. 281–287, 1988.
- [16] K. T. Small, "Single wire current share paralleling of power supplies," U.S. Patent 4717 833, 1988.
- [17] R. Wu, T. Kohama, Y. Koderu, T. Ninomiya, and F. Ihara, "Load-current-sharing control for parallel operation of dc-to-dc converters," in *IEEE Power Electronics Specialists Conf.*, 1993, pp. 101–107.
- [18] T. Kohama, T. Ninomiya, M. Shoyama, and F. Ihara, "Dynamic analysis of parallel module converter system with current balance controllers," in *1994 IEEE Telecommunications Energy Conf. Rec.*, pp. 190–195.
- [19] T. Kohama, T. Ninomiya, M. Wakamatsu, and M. Shoyama, "Static and dynamic response of a parallel-module high power-factor converter system with current-balancing controllers," in *IEEE Power Electronics Specialists Conf.*, 1996, pp. 1198–1203.
- [20] M. Jovanovic, D. Crow, and L. Fang-Yi, "A novel, low-cost implementation of 'democratic' load-current sharing of paralleled converter modules," *IEEE Trans. Power Electron.*, vol. 11, no. 4, pp. 604–611, 1996.
- [21] V. J. Thottuvelil and G. C. Verghese, "Stability analysis of paralleled dc/dc converters with active current sharing," in *IEEE Power Electronics Specialists Conf.*, 1996, pp. 1080–1086.
- [22] M. Youn and R. Hoft, "Analysis of parallel operation of inverters," in *IEEE Industry Applications Soc. Annu. Meet.*, 1976, pp. 951–958.
- [23] D. Maliniak, "Dense dc-dc converters actively share stress," *Electronic Design*, pp. 39–44, Jan. 1993.
- [24] M. Jordan, "UC3907 load share IC simplifies parallel power supply design," Unitrode Application Note U-129, Unitrode Corp., Merrimack, NH.
- [25] M. Chandorkar, D. Divan, and R. Adapa, "Control of parallel connected inverters in stand-alone ac supply systems," in *IEEE Industry Application Soc. Annu. Meet.*, 1991, pp. 1003–1009.
- [26] J. Bocek and C. Liu, "Determining current sharing criterion for parallel operation of power converters in multi-module bus systems," in *IEEE Power Electronics Specialists Conf.*, 1990, pp. 870–879.
- [27] J. Glaser and A. Witulski, "Output plane analysis of load-sharing in multiple-module converter systems," *IEEE Trans. Power Electron.*, vol. 9, no. 1, pp. 43–50, 1994.
- [28] R. V. White and F. M. Miles, "Principles of fault tolerance," in *IEEE Applied Power Electronics Conf.*, 1996, pp. 18–25.
- [29] R. L. Selders, "A current-balancing control system for cellular power converters," S.M. thesis, MIT, Cambridge, MA, 1996.
- [30] D. J. Perreault, K. Sato, and J. G. Kassakian, "Switching-ripple-based current sharing for paralleled power converters," in *Proc. Power Conversion Conf.*, Nagaoka, Japan, 1997, pp. 473–478.



Dr. Perreault is a Member of Tau Beta Pi, Sigma Xi, and the National Society of Professional Engineers.



Robert L. Selders, Jr. was born in Tacoma, WA, in 1970. He received the B.S. degree in electrical engineering from the Southern University and A&M College in 1993 and the S.M. degree in electrical engineering from the Massachusetts Institute of Technology, Cambridge, in 1996.

In 1996, he joined Delco Electronics Corporation, Kokomo, IN. He is currently engaged in the development and design of adaptive restraint technologies and systems for the supplemental inflatable restraint (SIR) Advanced Engineering Group.



John G. Kassakian (S'65–M'73–SM'80–F'89) received the Sc.D. degree from the Massachusetts Institute of Technology (MIT), Cambridge, in 1973.

He is a Professor of Electrical Engineering and Director for the MIT Laboratory for Electromagnetic and Electronic Systems. His fields of expertise are power electronics and automotive electrical systems, and he serves as a Consultant to government and industry. He has published extensively in the area of power electronics, and is a coauthor of the textbook *Principles of Power Electronics*.

Dr. Kassakian is the recipient of the IEEE Centennial Medal, the IEEE William E. Newell Award, the IEEE Distinguished Lectureship Award, and the Distinguished Service Award. He was the Founding President of the IEEE Power Electronics Society and serves as the U.S. representative to the European Power Electronics Society. In 1993, he was elected to the National Academy of Engineering.